JOURNAL OF COLLOID AND INTERFACE SCIENCE **186,** 53–59 (1997)
ARTICLE NO. CS964612

Entropic Contribution to the Retention of Nonspherical Particles in Field-Flow Fractionation

RONALD BECKETT*,[1] AND J. CALVIN GIDDINGS†

**CRC for Freshwater Ecology, Water Studies Centre and Department of Chemistry, Monash University, P.O. Box 197, Caulfield East, Vic., Australia 3145; and †Field-Flow Fractionation Research Center, Department of Chemistry, University of Utah, Salt Lake City, Utah 84112*

Received April 15, 1996; accepted September 16, 1996

In this paper the effect of particle shape on the entropy of nonspherical particles adjacent to a plane surface is considered. The subsequent influence on particle retention in field-flow fractionation (FFF) has been estimated. New retention equations for thin rod and disc shaped particles have been derived to cover this steric-entropic region of FFF. As particle size increases relative to the mean cloud thickness, the retention ratio for nonspherical particles is predicted to increase compared to small spherical particles of the same mass. This could result in a significant underestimation of the calculated equivalent spherical diameter (*d*) by FFF methods. The steric-entropic FFF equations could be used to calculate accurate *d* values if the large particle dimension is estimated independently (e.g., by microscopy). Alternatively, run conditions could be designed to minimize steric-entropic perturbations to the ideal retention equation.

Key Words: **field-flow fractionation; particle shape; particle size; FFF retention theory; nonspherical particles.**

INTRODUCTION

Field-flow fractionation (FFF) elution techniques are becoming widely accepted for their ability to achieve high-resolution separation and sizing of particles and macromolecules (1–6). A number of different subtechniques have been developed with a variety of capabilities. The subtechniques are based on the various fields and gradients that are used to cause selective transport and thus fractionation of the sample components as they are driven by flow through the ribbonlike FFF channel. The most commonly utilized of these subtechniques are sedimentation FFF (SdFFF), flow FFF (FlFFF), and thermal FFF (ThFFF), which are based on the application of gravitational or centrifugal acceleration fields, fluid flow, and thermal temperature gradients, respectively, perpendicular to the channel axis. The FFF separation mechanism is based on physical phenomena that easily lend themselves to rigorous mathematical analysis (modeling), enabling direct calculation of sample parameters from the measured retention time or volume (1, 2, 7).

The purpose of the field in FFF is to drive the suspended particles across the thin dimension of the channel toward one of the channel walls (the accumulation wall). In the normal mode of separation, particles are considered as small masses undergoing vigorous Brownian motion such that concentration diffusion balances the flux induced by the applied field driving the sample toward the accumulation wall. In these circumstances each sample component will achieve an equilibrium cloud structure adjacent to the accumulation wall which is characterized by an average cloud thickness *l*. Different components (consisting of particles of a given type and size) with different *l* values are then carried along the axis of the channel at unequal velocities by channel flow, leading to their separation. The unequal velocities arise because flow in the channel is parabolic and components with larger *l* values extend outward from the accumulation wall into faster streamlines of the parabola and thus experience a more rapid displacement downstream compared to particles with smaller *l* values (8).

The general mechanism described above is applicable when any type of field is used for the FFF separation of small particles. However, different fields respond differently to particle shape effects, which are a central issue to this work. In order to avoid confusion, our discussion and theoretical development will pertain specifically to sedimentation fields. We will mention later how results are expected to differ when other fields are applied.

For a sedimentation field, the equilibrium distribution of particles (and thus cloud thickness *l*) depends only upon the effective mass of the particles (particle mass minus buoyant mass) under consideration. For particles of equal density, *l* depends only upon absolute mass, particle volume, or equivalent spherical diameter. Particle shape effects do not enter into consideration. Thus the cloud thickness *l* and hence elution volume for normal mode FFF separations are usually considered to be independent of particle shape effects.

If the particle diameter is of the order of 1 μm or more, then Brownian diffusional displacements are reduced and the particle diameter becomes appreciable compared to the cloud thickness. Because the center of mass of the particle

[1] To whom correspondence should be addressed.

0021-9797/97 $25.00

is prevented from approaching the wall closer than allowed by the physical size of the particle, the mean particle position and thus its retention time is significantly perturbed by finite size effects, which we describe as steric effects. For the case of spherical particles the minimum approach distance is equal to the radius ($a(s)$) of the sphere. (The situation is more complicated for nonspherical particles.) This steric or wall exclusion effect causes particles to elute earlier than predicted by the ideal normal mode equations derived for point masses. The extreme case where $a(s) > l$ results in an inversion of the elution order in which the larger particles migrate through the FFF channel faster than smaller particles. This is referred to as the steric mode of FFF or simply steric FFF (1, 8).

A further complication is introduced by hydrodynamic lift forces which tend to elevate the particles above the accumulation wall, further perturbing their position and retention. The magnitude of the hydrodynamic lift forces increases with particle size (as well as with channel flow rates), again causing very large particles to elute before smaller ones (9). If particle elevation is sufficient, this mechanism leads to the lift-hyperlayer mode of FFF separation.

For either the steric or lift-hyperlayer mode, the mean distance of the particle center of mass above the accumulation wall (which controls particle retention) will vary markedly as the particle deviates from spherical shape. In the case of the steric phenomenon, the mean distance may be influenced by the nature of the particle motion. For example, elongated rods may either roll along the wall or they may tumble end-over-end in response to fluid shear forces. The type of motion would clearly influence mean particle position. Hydrodynamic lift forces are also known to depend on particle shape. For example, it has been shown that discs experience significantly larger hydrodynamic lift forces than spheres of the same volume (10).

We have noted that for spherical particles (or for any other particles with an aspect ratio near unity, such as blocky particles), there are two distinct retention domains, one corresponding to the steric mode where $a > l$ and the other described by the normal mode where $a < l$. (There is also a transition region in which both modes contribute significantly to retention.) This two-domain mechanism undergoes a fundamental change for particles of large aspect ratio, as considered here. Such particles can be considered to have two quite different dimensions which for convenience we label as a and a' where $a \gg a'$. The retention mechanism is now characterized by three distinct domains as described below:

$a' > l$	steric mode
$a > l > a'$	steric-entropic mode
$l > a$	normal mode

where again there are transition regions between. The purpose of this article is to describe the steric-entropic (alternately, sterentropic) mode and to develop theoretical expressions for retention in this mode and in the transition region between steric-entropic and normal modes.

The mechanism examined here for the steric-entropic mode is based on an entropic phenomenon in which entropy is reduced by any restriction in the possible rotational configurations of nonspherical particles as they approach within distance a of the accumulation wall. This is part of a general phenomenon in which it is thermodynamically less favorable for such particles to be located in close proximity to a surface as compared to being positioned more remotely from a surface where free rotation can take place (11, 12). It will be demonstrated that this loss of entropy can cause the cloud thickness to increase, thus resulting in a decrease in the retention volume. The above general effect will be illustrated by examining the predicted FFF elution behavior of thin rods and discs.

THEORY

FFF Retention Theory for Spherical Particles

The standard retention equation for normal mode FFF separations can be developed by considering an ensemble of point masses distributed in a potential energy gradient created by the applied field. Thermal energy tends to promote particles to regions of higher potential energy further removed from the accumulation wall. The equilibrium distribution is governed by the Boltzmann function. Thus the concentration $c(x)$ of particles at distance x from the accumulation wall of the channel will decrease exponentially according to the expression

$$c(x) = c_0 e^{-V(x)/kT} \qquad [1]$$

where c_0 is the particle concentration at the wall ($x = 0$), $V(x)$ is the potential energy of a single particle at distance x, k is Boltzmann's constant, and T is absolute temperature. If $V(x)$ is linear in x, $V(x) = -Fx$ where F is the force exerted by the field on the particle, then the dependence of concentration on distance x will be exponential as expressed by

$$c(x) = c_0 e^{-x/l} \qquad [2]$$

where $l = kT/|F|$. The exponential constant l is equal to the mean cloud thickness referred to earlier.

The fluid velocity profile across the channel is assumed to be parabolic and is thus given by

$$v(x) = 6\langle v \rangle \left(\frac{x}{w} - \frac{x^2}{w^2} \right) \qquad [3]$$

where $v(x)$ is the fluid velocity at distance x, $\langle v \rangle$ is the cross-sectional average linear fluid velocity, and w is the channel thickness.

The net migration of the component cloud is obtained by considering the integrated effect of the fluid velocity on the component concentration distribution. Displacement velocity is usually expressed in terms of the dimensionless retention ratio R

$$R = \frac{\langle V \rangle}{\langle v \rangle} = \frac{V^0}{V_r} \qquad [4]$$

in which $\langle V \rangle$ is the average component migration velocity, V_r is the sample elution volume, and V^0 is the channel void volume. The second equality of Eq. [4] holds only for constant field runs.

It can be shown that (8)

$$R = \frac{\langle c(x) \cdot v(x) \rangle}{\langle c(x) \rangle \cdot \langle v(x) \rangle}, \qquad [5]$$

or, in integral form,

$$R = \frac{w \int_0^w c(x) \cdot v(x) dx}{\int_0^w c(x) dx \cdot \int_0^w v(x) dx}. \qquad [6]$$

Integration using Eqs. [2] and [3] yields (8)

$$R = 6 \frac{l}{w} \left[\coth \frac{w}{2l} - \frac{2l}{w} \right], \qquad [7]$$

which in the limit when $l \ll w$ becomes

$$R = 6 \frac{l}{w} = 6\lambda, \qquad [8]$$

where the dimensionless term $\lambda = l/w$ is called the retention parameter. The above equations are applicable to small spherical or near-spherical particles provided the particle radius $a_s \ll l$.

For the case where a_s is appreciable relative to l, a correction for the steric effect is desirable. Giddings showed that this could be accounted for if l/w in Eq. [7] is replaced by $l/w(1 - 2a_s/l)$. In the limit of small l/w, this yields the approximate steric corrected normal mode retention equation (13)

$$R = 6 \frac{l}{w} + 6 \frac{a_s}{w}. \qquad [9]$$

Retention Theory for Nonspherical Particles

Consider a nonspherical particle with at least one dimension (a') small compared to l so that steric effects can be neglected. Let the longest dimension of the particle be $2a$ so that when the particle center of mass is less than distance a above the accumulation wall ($x < a$), there are some restrictions on the orientations that the particle can assume. This translates to a decrease in entropy $\Delta S(x)$ of the particle at any distance x compared to that for a spherical particle such that

$$\Delta S(x) = k \ln \frac{N_2}{N_1} \qquad [10]$$

where N_2/N_1 represents the ratio of the number of orientations that can be taken up by the nonspherical particle at a position $x < a$ to the number of orientations possible for an unrestricted sphere (at $x > a_s$). As pointed out by Gajdos and Brenner (12) this ratio can be equated to the ratio of the solid angle ($A(x)/A_s$) swept out by the appropriate vector which uniquely defines the orientation of the particle, to the solid angle for a complete sphere (4π). Thus we can rewrite Eq. [10] as

$$\frac{A(x)}{A_s} = e^{\Delta S(x)/k} = \alpha(x) \qquad [11]$$

where $A(x)$ is the area on the surface of a unit sphere swept out by the particle orientation vector in describing all of its allowed orientations and A_s is the total area of the unit sphere representing the unrestricted rotation of the particle.

The total free energy involved in elevating the particle a distance x above the wall in the presence of the field is thus $V(x) - T\Delta S(x)$, which on substitution for $V(x)$ into Eq. [1] yields

$$c(x) = c_0 e^{-V(x)/kT} \cdot e^{\Delta S(x)/k} \qquad [12]$$

Utilizing Eqs. [2] and [11] then gives

$$c(x) = c_0 e^{-x/l} \cdot \frac{A(x)}{A_s} = c_0 e^{-x/l} \cdot \alpha(x) \qquad [13]$$

The function $\alpha(x)$ depends on particle shape. For nonspherical particles $c(x)$ should approach zero for near-wall encounters (i.e., $c(o) = 0$) since when $x = 0$ only one unique orientation will be possible. Note that c_0 refers to the wall concentration of point masses which experience the same field force as the nonspherical particles under consideration. The particular expression for $c(x)$ derived from Eq. [13] can then be substituted into Eq. [6] to obtain the retention ratio. However, in this case the integrations must be performed in

two parts since the equation for $c(x)$ changes in form at $x = a$. Thus with nonspherical particles the analogous equation for R becomes

$$R = \left[w \int_0^a c_0 e^{-x/l} \cdot \frac{A(x)}{A_s} \cdot v(x)dx + w \int_a^w c_0 e^{-x/t} \cdot v(x)dx \right]$$

$$\left[\int_0^a c_0 e^{-x/l} \cdot \frac{A(x)}{A_s} dx + \int_a^w c_0 e^{-x/l} dx \right] \int_0^w v(x)dx \ . \quad [14]$$

This integration will yield an expression for R which depends on the combined values of a and l and reflects the near-wall orientation restriction weighted according to the relative time spent at each elevation (x value). The net result is an increase in R and corresponding earlier elution for the nonspherical particles compared to spherical particles with the same field interaction energy. This effect becomes more apparent as a increases relative to l.

RESULTS AND DISCUSSION

The utility of the above approach is best illustrated by taking some specific examples of commonly encountered particle shapes.

Application to Thin Rods

Consider a thin rod or needle of length $2a$ with center of mass at distance x above the accumulation wall as illustrated in Fig. 1(a). The unique orientation vector (magnitude = 1) lies along the needle axis and the area $A(x)$ is represented by the shaded region in Fig. 1(b). The solid angle for this situation is

$$\frac{A(x)}{A_s} = \frac{4\pi \sin\theta}{4\pi} = \frac{x}{a} \ . \quad [15]$$

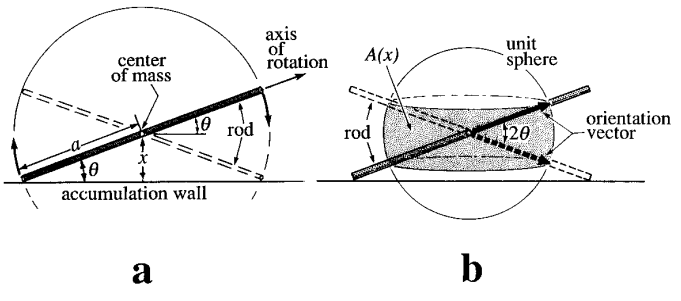

FIG. 1. (a) Representation of a thin rod of length $2a$ with center of mass at a distance x from the accumulation wall. Particle orientation is restricted to rotation of the particle by less than θ to the horizontal. (b) shows the area on the surface of the unit sphere swept out by the orientation vector (unit length). The area $A(x)$, used in defining the solid angle ($\alpha(x)$), is shaded.

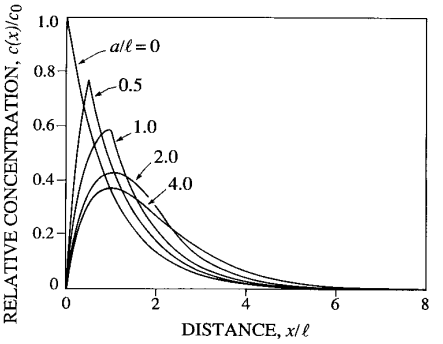

FIG. 2. Profiles of sample concentration ($c(x)/c_0$) versus relative distance from the accumulation wall (x/l) for the case of point masses ($a = 0$) and rods of length $2a$ with various a/l ratios.

Thus Eq. [12] becomes

$$c(x) = c_0 e^{-x/l} \cdot \frac{x}{a} \ . \quad [16]$$

The influence of the near-wall restriction on the particle concentration profile is illustrated by Fig. 2.

Substitution of Eq. [13] into Eq. [14] and performing the definite integrals yields

$$R = \frac{6l}{w} \left\{ \left[-1 - \frac{2l}{a} + \frac{a}{w} + \frac{4l}{w} + \frac{6l^2}{aw} \right] e^{-a/l} + \left[1 + \frac{2l}{w} \right] e^{-w/l} \right.$$

$$\left. + \left[\frac{2l}{a} - \frac{6l^2}{aw} \right] \right\} \Big/ \left\{ \left[\frac{l}{a} - \frac{l}{a} e^{-a/l} - e^{-w/l} \right] \right\} , \quad [17]$$

which on assuming both $l \ll w$ and $a \ll w$ simplifies to

$$R = \frac{6l}{w} \left[2 - \frac{a/l}{(e^{a/l} - 1)} \right] . \quad [18]$$

Two limiting forms of Eq. [17] are of importance. As $a/l \to 0$, $R \to 6l/w$ which is the same as obtained for an ideal point mass without considering particle shape (cf. Eq. [8]). When $a/l \to \infty$ (or $a \gg l$), then

$$R = 12 \frac{l}{w} = 12\lambda \quad [19]$$

representing a marked deviation from the ideal point mass retention value of $R = 6\lambda$. The complete retention behavior

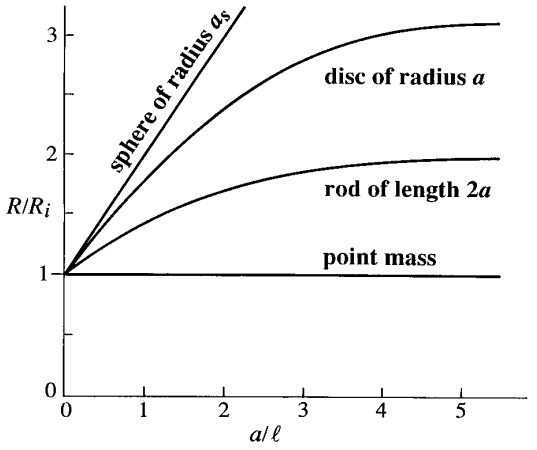

FIG. 3. Ratio of predicted retention ratio for finite particles (R) to ideal retention ratio (R_i) for point particles of equal mass. The simplified equations corresponding to $a \ll w$ and $l \ll w$ have been used. The ideal point mass value represented by the horizontal line at $R/R_i = 1$ contrasts with the increased retention ratio predicted for thin rods (Eq. [20]) and discs (Eq. [24]/Eq. [8]). For comparison the retention ratio expected for finite spheres of radius a (Eq. [9]) is also plotted.

of the thin rods is depicted graphically in Fig. 3. Here we divide Eq. [18] by Eq. [8] to obtain the ratio

$$\frac{R(\text{rod})}{R(\text{ideal})} = \left[2 - \frac{a/l}{(e^{a/l} - 1)}\right] \qquad [20]$$

and plot R(rod)/R(ideal) versus a/l. The retention behavior of the ideal point mass particles is represented by the horizontal line at R(rod)/R(ideal) = 1. The approximate retention behavior for finite spherical particles (of radius a_s), whose retention ratio (R(spheres)) is obtained using Eq. [9], is represented by the line on Fig. 3 which is a plot of R(sphere)/R(ideal) versus a_s/l. Note that both lines for the finite sized particles converge to a ratio of 1 as a/l approaches zero, but the limiting slope for the rods is less than that for a sphere. This is due to the fact that if we compare rods and spheres with $a = a_s$ the center of mass for the sphere is totally excluded from a layer closer than a_s from the wall but the rod can still take up orientations such that $x < a$, although as outlined in this paper there is still some entropic resistance to this occurring.

Application to Thin Discs

Next we will consider the case of a thin circular plate or disc of cross sectional radius a. Figure 4(a) shows the disc side on with its center of mass at distance x from the wall. The orientation of the disc is uniquely defined by a vector of unit length starting at the center of mass and directed at right angles to the disc plane as depicted in Fig. 4(b). The number of possible orientations of the disc in this situation is

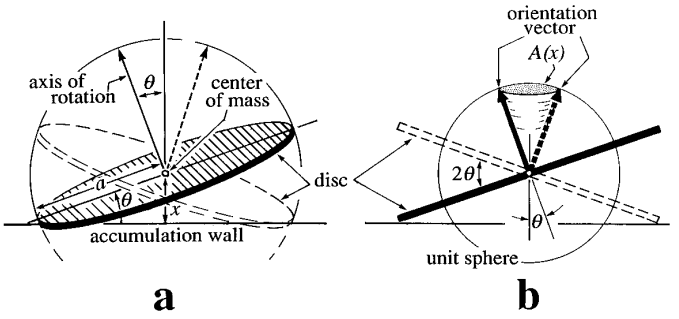

FIG. 4. (a) Representation of a thin disc of radius a with center of mass at distance x from the accumulation wall. Particle orientation is restricted to rotation of the disc by less than θ from the horizontal position. (b) shows the area on the unit sphere swept out by the orientation vector. The area $A(x)$, used in the calculation of the solid angle ($\alpha(x)$), is shaded.

represented by the shaded area that the end of the orientation vector transcribes in moving through all these configurations. This area must be doubled since the disc may also be inverted. The solid angle representing the orientation restriction due to position of the disc near the wall is thus

$$\frac{A(x)}{A_s} = \frac{4\pi(1 - \cos\theta)}{4\pi} = \left[1 - \sqrt{1 - \left(\frac{x}{a}\right)^2}\right]. \qquad [21]$$

Substitution into Eq. [13] gives

$$c(x) = c_0 e^{-x/l}\left[1 - \sqrt{1 - \left(\frac{x}{a}\right)^2}\right]. \qquad [22]$$

Some representative concentration profiles for discs are shown in Fig. 5.

The next step is to substitute Eq. [22] along with Eq. [3] into Eq. [14]. Unfortunately, the integrals involving the expression for $c(x)$ given in Eq. [22] cannot be performed analyt-

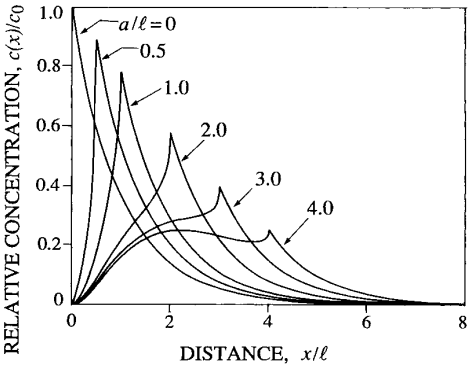

FIG. 5. Profiles of sample concentration ($c(x)/c_0$) versus relative distance from the accumulation wall (x/l) for the case of point masses ($a = 0$) and discs (of diameter $2a$) with various a/l values.

ically. However, we can pursue some approximations using series expansions of some of the terms in the equation which will lead to certain important limits of the expression for R.

Firstly, in order to explore the region where $a \gg l$ we replace the term $\sqrt{1 - (x/a)^2}$ in Eq. [22] by the Taylors series expansion with only two terms (i.e., $[1 - 1/2(x/a)^2]$) yielding

$$c(x) = \frac{1}{2}\, c_0 \cdot e^{-x/l} \cdot \frac{x^2}{a^2}\,. \qquad [23]$$

Substituting Eqs. [3] and [23] into Eq. [14], performing the definite integrals and simplifying by assuming both $a \ll w$ and $l \ll w$ produces

$$R \cong \frac{6l}{w}\left[\frac{3l^2}{a^2} + \left(\frac{a}{2l} - \frac{1}{2} - \frac{3l}{a} - \frac{3l^2}{a^2}\right)\Big/ e^{a/l}\right]\Big/\left\{\left[\frac{l^2}{a^2} + \left(\frac{1}{2} - \frac{l}{a} - \frac{l^2}{a^2}\right)\Big/ e^{a/l}\right]\right\}. \qquad [24]$$

Although this relationship is derived by integrating Eq. [23] from $x = 0$ up to a and the approximation is only valid for $x \ll a$, accurate values for R will result provided $l \ll a$. Under these conditions as x/a increases, giving rise to significant errors in the last term in Eq. [23], the exponential term approaches zero ensuring that these inaccurate regions do not contribute significantly to the overall integration.

The limit of this equation as $a/l \to \infty$ is

$$R = \frac{18l}{w} = 18\lambda. \qquad [25]$$

We note that this indicates an even greater deviation from the ideal point mass relationship (Eq. [8]) than for rods of the same major dimension (length $2a$) (see Eq. [17]). This is due to the fact that discs are more restricted in their motion on approaching a solid surface than rods which can rotate freely about their long axis. This results in a greater reduction in entropy for the discs than for rods and hence a bigger increase in the average cloud thickness.

It is also apparent that if $a \ll l$ the integrals over the range $x = 0$ to $x = a$ in Eq. [14] are small compared to those from $x = a$ to $x = w$. Thus as $a \to 0$ the expression for R approaches that given in Eq. [6] which reduces to $R = 6\lambda$. This is then the limiting R value for disc shaped particles as $a/l \to 0$. These trends are illustrated by the graph of R/R_i (i.e., Eq. [24] divided by $6l/w$) versus a/l given in Fig. 3.

CONCLUSIONS

Normal mode sedimentation FFF retention is generally thought to be independent of particle shape whereas for certain other FFF subtechniques, such as flow FFF where retention depends directly on the diffusion coefficient, some dependence on shape would be expected. We have extended the general retention equation for normal FFF to include a contribution due to entropy associated with the orientation of nonspherical particles. This involves computing the decrease in entropy due to the restriction on the particle orientation during near wall encounters. The addition to the particle free energy results in an expansion of the equilibrium sample cloud and a subsequent increase in the mean cloud thickness l, compared to that expected for small spheres of the same mass. Thus the retention time would be reduced and retention ratio increased. The theory has been used to derive new retention equations applicable to thin rods and discs with major length dimension of $2a$. In both cases the retention equations are the same as for small spheres (i.e., $R = 6\lambda$) provided $a \ll l$. However, when $a \gg l$ we obtain limiting forms of R(rod) $= 12\lambda$ and R(disc) $= 18\lambda$. This increased retention ratio could result in a considerable underestimation of the equivalent spherical diameter for highly retained nonspherical particles. This would be of considerable importance for many samples such as clay minerals.

The steric-entropic retention equations (e.g., Eq. [17] or [24]) could be used to calculate accurate equivalent spherical diameter data provided the large particle dimension (a) is measured independently (e.g., by microscopy) along with the FFF retention ratio (R). These quantities could be substituted and the relevant equation solved for the ideal cloud thickness (l) which then yields d. Alternatively, the steric-entropic equations could be used to design run conditions which would avoid a desired level of perturbation to the ideal retention equation.

We have observed significant shifts to larger retention ratios, for platey clay particles separated by sedimentation FFF, as the field is progressively increased and hence l is decreased (Tadjiki, Giddings, and Beckett, unpublished results). Although these shifts are about the same order as predicted by the steric-entropic theory, a lack of suitable well-characterized monodispersed nonspherical particle samples has hampered quantitative testing of the theory to date.

ACKNOWLEDGMENTS

We thank Mr. Soheyl Tadjiki for computing the concentration profiles given in Figs. 2 and 5 and Dr. Michel Martin for some helpful discussions on the manuscript. This work was supported by Grant CHE-9322472 from the National Science Foundation in the U.S.

REFERENCES

1. Giddings, J. C., *Science* **260,** 1456 (1993).
2. Giddings, J. C., and Caldwell, K. D., *in* ''Physical Methods of Chemistry'' (B. W. Rossiter and J. F. Hamilton, Eds.), Vol. 3B, Chap. 8, Wiley, New York, 1989.

3. Beckett, R., and Hart, B. T., *in* ''Environmental Particles'' (J. Buffle and H. P. van Leeuwen, Eds.), Vol. 2, Chap. 4, pp. 165–205. Lewis Press, Ann Arbor, MI, 1993.
4. Chittleborough, D. J., Hotchin, D. M., and Beckett, R., *Soil Sci.* **153,** 341 (1992).
5. Schimpf, M. E., *Trends Polym. Sci.* **1,** 74 (1993).
6. Beckett, R., Nicholson, G., Hotchin, D. M., and Hart, B. T., *Hydrobiologia* **235/236,** 697 (1992).
7. Giddings, J. C., Karaiskakis, G., Caldwell, K. D., and Myers, M. N., *J. Colloid Interface Sci.* **92,** 66 (1983).
8. Giddings, J. C., ''Unified Separation Science.'' Wiley, New York, 1991.
9. Williams, P. S., Lee, S., and Giddings, J. C., *Chem. Eng. Commun.* **130,** 143 (1994).
10. Beckett, R., Jiang, Y., Liu, G., Moon, M. H., and Giddings, J. C., *Part. Sci. Technol.* **12,** 89 (1994).
11. Giddings, J. C., Kucera, E., Russell, C. P., and Myers, M. N., *J. Phys. Chem.* **72,** 4397 (1968).
12. Gajdos, L. J., and Brenner, H., *Sep. Sci. Technol.* **13,** 215 (1978).
13. Giddings, J. C., *Sep. Sci. Technol.* **13,** 241 (1978).